Loss of Apc Rapidly Impairs DNA Methylation Programs and Cell Fate Decisions in Lgr5 + Intestinal Stem Cells

Marco Bruschi, Laure Garnier, Elouan Cleroux, Alicia Giordano, Michael Dumas, Anaïs Flore Bardet, Thomas Kergrohen, Stanislas Quesada, Pierre Cesses, Michael Weber, et al.

Loss of Apc Rapidly Impairs DNA Methylation Programs and Cell Fate Decisions in Lgr5^{+} Intestinal Stem Cells

Marco BRUSCHI[1], Laure GARNIER[1], Elouan CLEROUX[2], Alicia GIORDANO[1], Michael DUMAS[2], Anaïs Flore BARDET[2], Thomas KERGROHEN[3], Stanislas QUESADA[1], Pierre CESSES[1], Michael WEBER[2], François GERBE[1,*] and Philippe JAY[1,*]

[1]Institute of Functional Genomics (IGF), University of Montpellier, CNRS, INSERM, Equipe Labellisée Ligue Contre le Cancer, Montpellier, France

[2]UMR 7242 Biotechnology and Cell Signaling, CNRS, University of Strasbourg, 300 Bd Sébastien Brant, CS 10413, 67412 Illkirch, France

[3]Département de Cancérologie de l'Enfant et de l'Adolescent, Institut de Cancérologie Gustave Roussy, Université Paris-Sud, Université Paris-Saclay, 114 rue Édouard Vaillant, 94805, Villejuif Cedex, France

Running title: *DNA methylation changes drive intestinal tumor initiation*

*Corresponding authors: François Gerbe: +33-434-35-92-66, francois.gerbe@igf.cnrs.fr; Philippe Jay: +33-434-35-92-98, philippe.jay@igf.cnrs.fr; Institute of Functional Genomics, 141 rue de la Cardonille, 34094, Montpellier cedex 5, France

DISCLOSURE OF POTENTIAL CONFLICTS OF INTERESTS

The authors declare no competing financial interests.

Abstract

Colorectal cancer (CRC) initiation and progression result from the accumulation of genetic and epigenetic alterations. Although aberrant gene expression and DNA methylation profiles are considered hallmarks of CRC development, the precise timing at which these are produced during tumor establishment remains elusive. Here we investigated the early transcriptional and epigenetic changes induced by *Apc* inactivation in intestinal crypts. Hyper-activation of the Wnt pathway via *Apc* inactivation in crypt base columnar (CBC) intestinal stem cells (ISC) led to their rapid accumulation driven by an impaired molecular commitment to differentiation, which was associated with discrete alterations in DNA methylation. Importantly, inhibiting the enzymes responsible for *de novo* DNA methylation restored the responsiveness of *Apc*-deficient intestinal organoids to stimuli regulating the proliferation-to-differentiation transition in ISC. This work reveals that early DNA methylation changes play critical roles in the establishment of the impaired fate decision program consecutive to *Apc* loss-of-function.

Introduction

Although colorectal cancer (CRC) remains one of the leading causes of cancer-related death in developed countries (1), the mechanisms involved in its initiation remain only partially understood. The vast majority (80-90%) of CRCs is initiated by the constitutive activation of the Wnt pathway due to inactivating mutations in the *Adenomatous polyposis coli* (*APC*) tumor suppressor gene. Mouse models with germline or inducible *Apc* deletion recapitulate the early stages of tumorigenesis (2,3). In such models, adenomatous growth occurs upon bi-allelic mutation of *Apc* in the stem cell compartment, but not in differentiated cells, which are short lived, highlighting the key role of stem cells in tumorigenesis (4). Intestinal stem cells are intercalated between post-mitotic Paneth cells, which constitute the stem cell niche at the base

of crypts (5). *Apc* loss-of-function in those cells causes the formation of hypertrofic/hyperproliferative intestinal crypts with impaired epithelial organization (6,7). In both humans and mice, benign adenomas then progress toward malignant stages through the sequential accumulation of further genetic alterations (8–10). Beside those genetic alterations, the analysis of epigenetic profiles in CRC samples has initially revealed important remodelling of the DNA methylation profiles, distinguishing tumor tissues from their surrounding non-tumoral mucosa (11). Indeed, cancer cells display a general genomic hypomethylation, although genomic regions associated with tumor suppressors are frequently hypermethylated, which leads to their long-term transcriptional silencing (12). Recently, part of the alterations associated with CRC were shown to be already present in the intestinal adenomas found in Apc^{Min} mice, as compared to the surrounding non-transformed tissue (13). However, the extent and dynamics of DNA methylation changes occurring during early tumorigenesis, as well as whether they functionally contribute to tumor initiation, remain unclear. *De novo* patterns of methylation are established in unmethylated DNA regions by methyltransferases DNMT3A and DNMT3B, and then maintained through cell divisions by DNMT1 (14). Importantly, *de novo* methyltransferases are preferentially expressed in the epithelial proliferative crypt compartment and overexpressed in tumor samples (15), and their activity was reported to promote adenoma formation through the methylation of specific loci (16–18). Importantly though, all these comparisons have been based on heterogenous biological samples (i.e. cancer samples at various stages vs. non-transformed mucosa) in which the proportions of the different cell types are significantly altered, whereas transcriptomic programs and DNA methylation profiles can vary extensively during cell differentiation, including in the intestinal epithelium (15,19–25). Here, we investigated the earliest consequences of the loss of *Apc* function specifically in the predominant tumor cells-of-origin expressing the *Leucine Rich Repeat Containing G Protein-Coupled Receptor 5* (*Lgr5)* CBC stem cell marker, early after the induction of *Apc* deletion. We

then exploited the organoid culture system to dissect further the functional role of DNA methylation variations during the early tumorigenic process.

Materials and Methods

Extended experimental procedures are described in the Supplemental Information.

Animal strains and procedures. All animal experiments were approved by the French Agriculture and Forestry Ministry. All the mice were on a C57BL/6/J genetic background and maintained in an SPF animal facility.

Flow cytometry, fluorescence-associated cell sorting and cell cycle analyses. Single cell suspensions of the most proximal 1/3 of freshly isolated small intestine were used for the cell cycle analysis or FACS sorting of GFP^+ cells directly in RLT+ lysis buffer (Qiagen) for subsequent gDNA/RNA extraction, using a FACSAria (Becton Dickinson). Flow cytometry analyses were performed by using the FlowJo software (FlowJo LLC).

Organoid formation assay and organotypic culture methods. Culture of organotypic structures from Lgr5-GFP^+ cells or intestinal crypts was performed as previously described(26). To induce the Cre-mediated recombination of *Apc in vitro,* cells were cultured during 3 days in a medium supplemented with 4-OH-tamoxifen (200 nM) resuspended in ethanol. To inhibit the activity of DNA methyltransferases, medium was supplemented with Nanaomycin-A (5µM) reconstituted in DMSO or 5-Azacytidine (200 nM) (Sigma-Aldrich) administered at the same time than 4-OH-tamoxifen treatment and then maintained all along the culture. Lentiviral-mediated transduction and antibiotic selection were performed as previously described (27), with minor modifications. Experimental procedures for the evaluation of growth kinetics, clonogenic potential and responsiveness to R-spondin depletion or BMP stimulation are detailed in the supplemental information.

gDNA and RNA methods. DNA and RNA of FACS-sorted eGFP$^+$ cell and intestinal organoids were isolated using the Allprep DNA/RNA Micro (GFP$^+$ cells) or Mini (organoids) kit (Qiagen) according to the manufacturer's instructions and used for next generation sequencing, RT-PCR, RT-qPCR and McrBC-qPCR methylation assay.

Data Access. The accession number for the sequencing data reported in this work is GenBank: GSE123006

Fluorescent immunohistochemistry on paraffin-embedded tissue and organotypic cultures. Tissue dissection and immunohistochemistry on 5-µm-thick sections of paraffin-embedded tissue and organotypic cultures were performed essentially as described previously (28) . All experiments were performed on formalin-fixed tissues with epitope retrieval in boiling 10 mM sodium citrate (pH 6.4).

Results

Apc loss-of-function leads to the expansion of the Lgr5$^+$ stem cell compartment without increasing the rate of stem cell division.

To investigate the cellular and molecular dynamics of the ISC compartment during early tumorigenesis, we used the *Lgr5-Cre^{ERT2}-ires-eGFP* mouse line that allows specific identification and genetic manipulation of the intestinal CBC stem cell population (29). In this model, the variegated expression of the eGFP and the Cre^{ERT2} recombinase leads to two distinct populations of intestinal crypts, expressing or not the knocked-in allele under the control of the *Lgr5* promoter. When in combination with *Apc$^{LoxP/+}$* or *Apc$^{LoxP/LoxP}$* alleles, the administration of tamoxifen results in deletion of one or both *Apc* alleles in *Lgr5*-expressing ISCs. Such recombined ISCs will be called hereafter *Apc^{HET}* and *Apc^{KO}*, respectively, whereas non-recombined ICSs will be named *Apc^{WT}*. As early as fifteen days after tamoxifen administration, the loss of a single *Apc* allele did not produce significant changes in the size of the eGFP$^+$ stem/progenitor cell compartment, whereas the biallelic loss, resulting in Wnt activation in most

of the GFP-expressing intestinal crypts, produced a mean 9-fold expansion of eGFP$^+$ cells as compared to *Apc*^{WT} controls (Fig. 1A, B). Consistently with this observation, a clonogenic assay performed by seeding FACS-sorted eGFP$^+$ cells led to the development of significantly more multicellular organotypic structures from *Apc*^{KO} eGFP$^+$ cells as compared to *Apc*^{WT} eGFP$^+$ cells, thus confirming the increased proportion of eGFP$^+$ cells endowed with stem ability in *Apc*^{KO} crypts. (Fig. 1C). Indeed, we observed an increase in the number of cells expressing the *bona fide* ISC marker Olfm4 in *Apc*^{KO} crypts compared to their *Apc*^{WT} counterparts (Fig. 1D), as well as cells expressing Sox9 (Fig. 1E), a marker shared by ISCs and Paneth cells in the intestinal epithelium. Moreover, quantification of eGFP$^+$ ISCs on intestinal sections using the very restrictive anatomic criterion of a direct contact with the Lyzozyme-expressing Paneth cell niche denoted an accumulation of ISCs following *Apc* deletion, associated with the concomitant increase of Paneth cell numbers in *Apc*^{KO} crypts (Supplementary Fig. S1 A, B). Together, these results indicate that *Apc* inactivation induces a rapid expansion of the ISC compartment.

The Wnt signaling pathway is considered as a major driving force of intestinal epithelial proliferation. Accordingly, deletion of its transcriptional effector *Tcf7l2/Tcf4* causes proliferation arrest whereas aberrant constitutive activation of the Wnt pathway following *Apc* loss-of-function results in the accumulation of proliferating cells and formation of hypertrophic crypts (30,31). As expected, *Apc*-deficient ISCs gave rise to crypts with increased numbers of actively proliferative BrdU$^+$ cells (Fig. 1F-G). To evaluate the direct contribution of ISCs proliferation in the expansion of *Apc*-deficient crypts, we assessed the cell cycle status of ISCs following *Apc* deletion. Surprisingly, the incorporation of BrdU after a pulse of 2 hours (Fig. 1F) indicated a slight but significant reduction of BrdU$^+$ eGFP$^+$ cells upon deletion of *Apc* (Fig. 1H), instead of an increased proliferation of *Apc*^{KO} ISCs. We confirmed that *Apc* deletion is not directly linked to increased proliferation rates in ICSs by flow cytometry quantification of the proportion of eGFP$^+$ cells found in the S phase using propidium iodide staining of cellular

DNA (Fig. 1I). In addition, no significant difference was found between numbers of Apc^{KO} and Apc^{WT} BrdU$^+$ cells when we only considered ISCs, defined as eGFP$^+$ cells in direct contact with Lyz$^+$ Paneth cells (Fig. 1J). Of note, the proportion of eGFP$^+$ cells expressing markers of terminal differentiation into Paneth (Lyz$^+$), enteroendocrine (Chga$^+$) or tuft (Dclk1$^+$) post-mitotic cell lineages was slight (<3%) for both genotypes (Supplementary Fig. S1C-F). Moreover, analysis of the post-mitotic tuft cell surface marker Siglec-F (Supplementary Fig. S1G), revealed a physiological representation of tuft cells (~0.4%, Supplementary Fig. S1H) within the epithelial samples, with minimal and comparable co-localization of this marker with eGFP in Apc^{WT} and Apc^{KO} sorted cells (Supplementary Fig. S1I). Together, these data rule out the possibility that the increased proportion of non-dividing cells in the total Lgr5-GFP$^+$ Apc^{KO} compartment may reflect a larger proportion of terminally differentiated cells with residual eGFP protein with our cell-sorting strategy. We thus concluded that *Apc* deletion causes the accumulation of eGFP$^+$ cells with ISC features in Apc^{KO} intestinal crypts, which cannot be ascribed to an augmented rate of cell division in ISCs.

ISC accumulation following *Apc* loss-of-function relies on an impaired molecular commitment towards differentiation.

To identify the mechanisms underlying the rapid ISC accumulation following *Apc* loss-of-function, we next investigated the molecular consequences associated with *Apc* disruption, specifically in eGFP$^+$ cells comprising ISCs and their most direct progeny in the transit-amplifying (TA) crypt compartment. The comparison of gene expression profiles of Apc^{WT} and Apc^{HET} FACS-sorted eGFP$^+$ cells by RNA-seq showed that the first genetic hit in the *Apc* locus, i.e. the loss of a single *Apc* allele (Apc^{HET}), significantly altered the expression of more than 400 transcripts (FDR-adjusted p<0.01) as compared to Apc^{WT} eGFP$^+$ cells (Fig. 2A, results listed in table S1).

Quantification of the residual loxP-flanked exon-15 showed an average 83% reduction of this exon in cells from *Apc*$^{LoxP/LoxP}$;*Lgr5-Cre*^{ERT2} (*Apc*^{KO}) mice (Supplementary Fig. S2A), therefore confirming the efficient loss of the full-lenght *Apc* transcript in the majority of sorted cells in our experimental setting. Remarkably, such a biallelic disruption of *Apc*, resulting in constitutive Wnt activation, caused dysregulation of approximately 5000 transcripts (Fig. 2A) in *Apc*^{KO} eGFP^{+} cells, highlighting a dramatic rewiring of gene expression in ISCs and their immediate progeny associated with the constitutive activation of Wnt signaling. Remarkably, a subset of genes was exclusively expressed in either one or the other genetic condition. Among these markers, the endoderm-specific *SRY-box 17* (*Sox17*) transcription factor (Supplementary Fig. S2B) was undetectable in both *Apc*^{WT} and *Apc*^{HET} eGFP^{+} cells and expressed in *Apc*^{KO} eGFP^{+} cells. Immunohistochemical detection confirmed that this gene is ectopically expressed by scattered *Apc*^{KO} eGFP^{+} cells within the ISC zone as early as day 6 post-recombination, and then intensely expressed in the transit amplification compartment of *Apc*^{KO} crypts (Supplementary Fig. S2C).

To gain further insight into the changes occurring upon the disruption of *Apc* in ISCs we performed gene set enrichment analyses (GSEA). The analyses on the representation of wide collections of gene sets related to chemical and genetic perturbations (*c2.cgp.v6.1*) and KEGG pathways (*c2.cp.kegg.v6.1.symbols*) in *Apc*^{WT} and *Apc*^{KO} gene expression profiles revealed an overlap with the results from other studies on the outcome of *Apc* inactivation in mouse models of early tumorigenesis and human adenomas (reported in Tables S2,S3; examples of sets related to early tumorigenesis are shown in Supplementary Fig. S2G). Consistently with *Apc* abrogation, GSEA interrogation of our data confirmed an exacerbated Wnt signaling in *Apc*^{KO} eGFP^{+} cells, with an increased expression (negative correlation with *Apc*^{WT} gene expression, NES WT vs KO=-1.57) of the set of genes representing β-catenin transcriptional targets (Fig. 2B). In line with the cell cycle analyses of ISCs from *Apc*^{WT} or *Apc*^{KO} mice, indicating absence

of increased cell proliferation (Fig. 1D-F), no preferential enrichment was found in Apc^{KO} or Apc^{WT} eGFP^{+} cell profiles for the set of genes associated with progression through the cell cycle (Fig. 2B). Concomitantly, the gene signature associated with ISC identity (32) (Table S4) showed a significant enrichment (NES WT vs KO=-1.6) in the transcriptomic profiles of Apc^{KO} eGFP^{+} cells (Fig 2B). Conversely, the signature associated with intestinal epithelial differentiation (33) was depleted in the gene expression profiles associated with Apc^{KO} cells (Fig 2B, NES WT *vs* KO =2.95), whereas no significant enrichment was detected for the set of genes associated with progenitor cells from the transit-amplification compartment in one or the other conditions (Fig. 2B). Indeed, a subset of *bona fide* ISC markers, including *Lgr5*, *Axin2, Musashi RNA Binding Protein 1* (*Msi1*), and others, were up-regulated in Apc^{KO} eGFP^{+} cells (Fig. 2C), whereas early markers of intestinal epithelial commitment (*Atoh1*, *Spdef*) and differentiation into enterocytes (*Elf3*, *Krt20*), goblet (*Cdx2*, *Muc2*), enteroendocrine (*Insm1, Chga*), tuft (*Pou2f3*, *Dclk1*) and M (*Spi-B*) epithelial cell lineages were down-regulated (Fig. 2D). The most important exception was represented by markers associated with Paneth cell maturation, which is known to rely on Wnt signaling (7,34). Indeed, we could observe the expression of transcription factors involved in lineage commitment in eGFP^{+} CBC cells and, more frequently, in eGFP^{+} cells immediately above the CBC cell zone in control mice (Fig. 2E-H). We found Apc^{WT}-eGFP^{+} cells clearly expressing markers involved in lineage commitment such as Elf3 (an enterocyte specification marker (35)) and Cdx2 (a pan-epithelial marker involved in enteroendocrine cell commitment (36)) or, less frequently, Insm1 (enteroendocrine cells (37)) or Pou2f3 (tuft cells specification (38)). Overall, the expression of these markers in the self-renewal compartment supports the early lineage specification occurring in ISCs and their daughter TA cells, which is impaired by the inactivation of the gate-keeper *Apc* gene.

We then decided to examine the possible involvement in these findings of the transcriptional regulator *Myc*, an important Wnt target gene previously described as a key mediator of the

epithelial phenotype consequent to *Apc* loss (39,40). As expected, the size of the Myc^{+} compartment expanded during time following *Apc* inactivation, as *Myc* was expressed by the increasing number of cells showing β-catenin translocation in Apc^{KO} crypts compared to Apc^{WT} control crypts (Supplementary Fig. S2D). However, constitutive activation of Wnt signaling in Apc^{KO} Lgr5-GFP cells did not further increase the expression of *Myc* in individual FACS-sorted stem/progenitor cells (Supplementary Fig. S2E). Together, these observations suggest that the specific effects of *Apc* loss and exacerbated Wnt signaling found in ISCs do not rely on an altered level of *Myc* expression. Interestingly, the expression of the Myc paralogue Mycn, which is known to be preferentially expressed by differentiated cells in the intestinal epithelium (39), was significantly reduced in Apc^{KO} cells (Supplementary Fig.S2F). Overall, these results revealed that the primary outcome of the oncogenic Wnt pathway hyper-activation in Apc^{KO} ISCs consists in their impaired commitment toward differentiation, which explains their rapid accumulation in spite of the absence of increased ISC division rate.

Exacerbated Wnt activation is accompanied by rapid and defined alterations in the DNA methylation of the self-renewal compartment.

We then investigated if the impairment in the ability of *Apc*-deficient ISCs to commit toward differentiation is accompanied by rapid alterations of DNA methylation profiles. Some instructive changes in the DNA methylation patterns have been shown to occur during homeostatic intestinal differentiation (15,25). Moreover, alterations in the DNA methylation patterns have been reported in advanced stages of CRC and, more recently, in early adenomas (11–13,41,42). However, whether these alterations are immediate consequences of the oncogenic loss of *Apc* function remains unclear. We therefore performed reduced-representation bisulfite sequencing (RRBS) on FACS-sorted Apc^{WT}, Apc^{HET} and Apc^{KO} $eGFP^{+}$ cells. Hierarchical clustering of the methylation scores provided fair discrimination of the

257 Apc^{KO} from the Apc^{WT} and Apc^{HET} samples, indicating a specific impact of *Apc* inactivation on
258 the methylome (Fig. 3A). Overall, RRBS analyses revealed significant discrete rearrangements
259 of the DNA methylation profiles in Apc^{HET} and Apc^{KO} eGFP^{+} cells as compared to Apc^{WT}
260 controls (Fig. 3B). We identified 58 differentially methylated regions (DMRs) in Apc^{HET} eGFP^{+}
261 cells compared to eGFP^{+} cells from control mice, and 790 DMRs in Apc^{KO} eGFP^{+} cells (detailed
262 in Table S5). In line with the notion of a general DNA hypomethylation in CRC samples
263 (11,12), 75% of the DMRs were hypomethylated in Apc^{KO} cells (Fig. 3C). These DMRs were
264 reproducible between replicates, highlighting the consistent effect exerted by *Apc* loss on the
265 DNA methylation profiles (Fig. 3D). Both hypo- and hypermethylated DMRs identified by
266 RRBS were generally distant from gene transcription start sites (TSSs), with only 57 out of 790
267 DMRs located within 2000 bps from the most proximal TSSs (Fig. 3E), and are preferentially
268 located within intronic and inter-genic regions (Supplementary Fig. S3A). This is in accordance
269 with previous findings obtained by comparing the DNA methylation in adenoma samples and
270 in ISCs (42). Importantly, the DNA methylation changes occurring 15 days after *Apc* deletion
271 remained focal and less extensive than the general DNA remodeling described in colon cancer
272 (11,41). For instance, repeated elements belonging to endogenous retrotransposon families,
273 such as intrascisternal-A-particles (IAPs), are severely methylated in normal cells and
274 frequently hypomethylated in cancer cells (43,44). However, the methylation of these regions
275 was not affected 15 days following Wnt constitutive activation (Fig. 3F). This result was
276 confirmed experimentally for IAPs by qPCR on genomic DNA fragments obtained after
277 digestion with the McrBC methylation-sensitive restriction enzyme (Supplementary Fig. S3B).
278 Taken together, these observations indicate that the DNA methylation status of a defined subset
279 of genetic loci changes very rapidly at tumor initiation following loss of *Apc* function.
280 To investigate the direct involvement of altered DNA methylation in the impaired ability of
281 ISCs to commit towards differentiation we first interrogated the RRBS profiles for the

enrichment of epithelial stem and post-mitotic signatures (Tables S4), by analyzing the methylation of promoter regions (encompassing -1000 bps to +500 bps from the TSS). GSEA results did not show global tendencies in the methylation of the TSSs associated to genes belonging to those sets (Fig. 3G). Even restricting the analysis to the list of TSSs associated with the identified DMRs (Tables S5) did not show preferential hypermethylation of genes associated with post-mitotic commitment (Fig. 3G), therefore indicating that altered DNA methylation of loci directly associated with stemness/maturation does not represent an instructive mechanism for the imbalanced fate program dictated by *Apc* loss. As ISC identity and commitment are regulated by opposite gradients of Wnt and BMP/TGF-β signaling along the crypts-villus axis (a schematic representation is provided in Supplementary Fig. S3C), we focused our attention on these two signaling pathways. Indeed, secretion of Wnt ligands and BMP/TGF-β inhibitors co-operate to the formation of a stem-permissive niche in both homeostatic crypts and adenomas (45–47). Thus, forcing BMP inhibition concomitantly to Wnt constitutive activation leads to the expansion, or even to the ectopic formation of an adenoma stem cell compartment (48,49), whereas increasing secretion of BMP ligands along the villus axis was shown to promote epithelial differentiation (46). Combining the data from RRBS and RNA-seq analyses revealed an altered extent of methylation and expression of four loci associated to components of the Wnt pathway (*Axin2*, *Nfatc2*, *Prkca*, *Vangl1*) and three loci associated with the TGF-β/BMP signaling pathway (*Inhbb*, *Bmp7*, *Smad6*) in Apc^{KO} $eGFP^{+}$ cells (Supplementary Fig. S3D, E). The *Smad6* locus, coding for an intracellular inhibitor of the BMP signaling pathway, was used for experimental validation using gDNA and RNA samples from an independent cohort of Apc^{WT} and Apc^{KO} $eGFP^{+}$ cell samples from intestinal epithelia. McrBC-qPCR and RT-PCR analyses confirmed the hypomethylation (Supplementary Fig. S3F) and increased expression (Supplementary Fig. S3G) of Smad6 in Apc^{KO} ISCs.

Overall, these observations suggested that rapid, defined, changes in the methylation patterns of specific loci may be implicated in impaired cell fate decisions at tumor initiation.

Inhibition of *de novo* DNA methyltransferases partially compensates the consequences of constitutive Wnt signaling after *Apc* inactivation in intestinal organoids.

We next evaluated the contribution of DNA methylation changes in the altered behaviour of Apc^{KO} ISCs. We first re-assessed the expression patterns of *de novo* methyltransferases Dnmt3a and Dnmt3b in the normal and Apc^{KO} epithelium. RNAseq data showed no significant differences in the expression of Dnmt3a between Apc^{WT} and Apc^{KO} Lgr5-GFP cells (4A), whereas the expression of Dnmt3b was slightly but significantly increased upon *Apc*-loss in those cells (4C), probably reflecting ISC accumulation within the compartment. Specific immunostainings confirmed that these enzymes are preferentially expressed in the in normal intestinal crypts, with Dnmt3a signal spanning from ISCs to TA cells at crypt/villus border, whereas Dnmt3b staining was accentuated in ISCs and immediate daughter cells in the normal crypt (Fig 4B and 4D, upper panels). Those patterns were clearly expanded upon *Apc* deletion in transgenic crypts, in accordance with the outgrowth of cells displaying β-catenin translocation (4B, 4D central panels). Furthermore, these enzymes were expressed in virtually all Apc^{KO} epithelial cells in well-developed adenomas from $Apc^{\Delta 14/+}$ mice harbouring a germline heterozygous mutation on *Apc*, and spontaneously developing clonal adenomas from stem cells in which the remaining wild type *Apc* allele has been mutated or silenced (bottom panels). Having shown that the dynamics of *de novo* Dnmt patterns coincide with the expansion of the intestinal self-renewal compartment, we then investigated whether the precocious changes in DNA methylation that we observed in ICSs following constitutive Wnt activation are functionally involved in such an expansion at the expense of homeostatic commitment to differentiation. To this end, we assessed the outcome of *de novo* methyltransferases inhibition

in intestinal organotypic cultures (organoids) derived from the intestinal epithelium of $Apc^{LoxP/LoxP}$;$VillinCre^{ERT2}$ mice. Such organoids are normal (Apc^{WT}) until they are treated with tamoxifen, which results in the deletion of both *Apc* alleles (Apc^{KO}) in all epithelial cells. RT-qPCR quantification confirmed a substantial reduction (>400-fold change) in the LoxP-flanked exon-15 upon treatment with 4-OH-tamoxifen, therefore validating the effective abrogation of the functional full-length *Apc* transcript (Supplementary Fig. S4A). Indeed, we constantly observed a switch toward a spheroid morphology (Supplementary Fig. S4B), an increased proportion of actively proliferating ($Ki67^+$) cells (Supplementary Fig. S4C) consistent with increased global crypt proliferation in mice (see Fig. 1G), overall confirming the Wnt oncogenic activation in Apc^{KO} intestinal organoids. All those phenotypic changes were associated to the accumulation of cells expressing the ISC maker Sox9 (Fig. 4E) in Apc^{KO} organoids, which is consistent with the increased stemness described in the figure 1.

$Apc^{LoxP/LoxP}$;$VillinCre^{ERT2}$ organoids were lentivirally transduced with shRNAs directed against *Dnmt3a* and *Dnmt3b* transcripts or, as a control, with lentiviral vectors containing length-paired non-target sequences. Immunohistochemical detection confirmed the reduced amount of nuclear Dnmt3a and Dnmt3b enzymes (Supplementary Fig. S4D-E). The knock-down of the two enzymes did not affect the general rate of proliferation of Apc^{WT} models (total average of $59.9\% \pm 7.1$ vs. $51.2\% \pm 5.70$ of $Ki67^+$ cells in replicates from two NT-control and two double-sh clones respectively, Fig. 4F). As expected, after *Apc* deletion the general extent of cell proliferation was increased in control organoids expressing non-target shRNAs (total average of $77.1\% \pm 2.5$ in two clones). In sharp contrast, the combined knock-down of Dnmt3a/Dnmt3b reduced the general proliferation of Apc^{KO} organoids to an extent comparable to Apc^{WT} organoids (total average of $53.9\% \pm 3.4$ in two clones, Fig. 4F), supporting the notion of a requirement of *de novo* methyltransferase function in the phenotype resulting from *Apc* loss-of-function. Compared to Apc^{KO} organoids transduced with non-target shRNA, Apc^{KO}

organoids with Dnmt3a/Dnmt3b knock-down also displayed a reduced sphere formation ability in 3/3 replicates when replating was performed by dissociating a number of organoids equivalent to an identical number of cells (Fig. 4G), therefore suggesting a decreased stemness, as defined by the ability of a single cell to proliferate and generate a multicellular organoid, of Apc^{KO} organoid cells with reduced Dnmt3a/b expression. To confirm these findings with an independent approach, we tested the effect of *de novo* methyltransferases inhibition by treating organoids with the specific Dnmt3b inhibitor Nanaomycin-A, or with the demethylating agent 5-Azacytidine (50). Remarkably, the administration of either inhibitor concomitantly with the deletion of *Apc* resulted in reduced proliferation rates in three independent organotypic models (Fig. 4H), at extents comparable to those of isogenic Apc^{WT} organoids, in which cell division rate was not affected by the presence of inhibitors, although increased cell-death was observed early after administration of 5-Azacytidine. Moreover, when we examined the expression of Wnt-related genes (*Axin2*, *Nfatc2*, *Prkca* and *Vangl1*) and BMP-related genes (Smad6, Inhbb and Bmp7) that were differentially methylated and expressed in Apc^{KO} CBC (see figure S3D-E), we found that those genes were also differentially expressed in Apc^{KO} organoids compared to Apc^{WT} controls (figure 4I), thus confirming the relevance of organotypic models in the study of homeostatic disruption upon *Apc* inactivation. Taken together, these results indicate that the activity of *de novo* methyltransferases is required for the increase in the proportion of actively proliferating cells able to form growing organoids following *Apc* loss-of-function.

De novo DNA methyltransferase activity contributes in altering Wnt and BMP signaling driving ISC accumulation upon _Apc_ inactivation.

Next, we sought to test whether *de novo* methyltransferase activity is implicated in the responsiveness of Apc^{KO} epithelial cells to environmental Wnt and BMP stimuli, regulating the homeostatic choice between self-renewal and differentiation. Intestinal organoids are routinely

maintained in presence of R-spondin 1 (Rspo), which cooperates with Wnt signals to define ISC properties (51), and becomes dispensable following constitutive Wnt activation (26,52). Indeed, we observed a loss of spheroid formation ability and reduction of spheroid size in Apc^{KO} organoids with combined *Dnmt3a* and *Dnmt3b* knock-down. Strikingly, these effects were further accentuated upon withdrawal of Rspo from the culture medium (Fig. 5A, B). This confirmed the reduction in the sphere-formation ability and proved the recovered dependence to Rspo upon *de novo* Dnmts knock-down in Apc^{KO} organoids. We then assessed the responsiveness of Apc^{KO} organoids to the stimuli that modulate the BMP signaling. Stimulation of organoid cultures with recombinant BMP2 after withdrawal of the BMP inhibitor Noggin from the medium dramatically increased the formation of crypt-like structures in *Dnmt3a*/*Dnmt3b* shRNA-expressing Apc^{KO} organoids as compared to the non-target shRNA control Apc^{KO} organoids (Fig. 5C). This indicated a restauration of the ability of epithelial cells to morphologically self-organize the formation of distinct crypt and differentiated compartments. Indeed, control individually seeded Apc^{KO} cells were largely more prone to form spheroids than Nanaomycin-A-treated cells in the presence of rBMP2 stimulation (Fig. 5D), supporting the recovered responsiveness to differentiation stimuli orchestrated by BMP signaling upon *de novo* Dnmt inhibition. As in the case of FACS-sorted $eGFP^{+}$ cells from Apc^{WT} and Apc^{KO} crypts (Supplementary Fig. S3E), Apc^{KO} organoid cultures displayed an upregulation of the BMP inhibitor *Smad6* mRNA as compared to Apc^{WT} organoids. Moreover, treatment with 5-azacytidine reduced the expression level of this gene in 2/2 independent Apc^{KO} organoid cultures (Supplementary Fig. S5A) and Nanaomycin-A exerted comparable effect in 2/3 independent cultures (Supplementary Fig. S5B). To further elucidate the responsiveness to BMP signaling as involved in the *Apc* phenotype, we therefore decided to test the implication of the Alk-pSmad axis physiologically regulated by Smad6 during homeostasis. Strikingly, BMP inhibition resulting from the addition of the Alk-pSmad inhibitor LDN193189 abolished

406 the rescue exerted by Dnmt3b inhibition mediated by Nanaomycin-A treatment, as
407 demonstrated by the size (Fig. 5E-F, quantification from two independent models) and
408 proliferative rate (Supplementary Fig S5C) of spheroids compared to controls and Nanaomycin-
409 A treated organoids. Together, these results confirm that *de novo* DNA methylation occurring
410 upon *Apc* inactivation is critically involved in the increase in the proportion of actively
411 proliferating cells within the intestinal epithelium by dictating a reduced responsiveness of ISCs
412 to the different stimuli regulating the proliferation-to-differentiation balance (summarized in
413 Fig. 5G).
414

415 **Discussion**

416 We investigated the early consequences of oncogenic *Apc* loss-of-function, the most common
417 genetic initiating event in CRC, on the behavior of ISCs. Importantly, we show that this tumor
418 suppressor does not operate by negatively controlling the rate of cell division of intestinal stem
419 cells but rather represents a critical regulator of the ability of ISCs to engage towards
420 differentiation. In line with the rapid accumulation of ISCs observed early upon *Apc* deletion,
421 the analysis of ISC gene expression profiles clearly confirmed the impaired ability of stem cells
422 and their progeny to commit toward homeostatic differentiation, with a reduced expression of
423 several markers for the different post-mitotic cell lineages. Recently, single cell RNA-seq
424 analyses from purified $Lgr5^{+}$ cells revealed a relatively homogeneous stem cell population
425 mixed with rare secretory cells, likely reflecting early fate commitment decision in some
426 progenitor cells (53). Indeed, we show that some markers of lineage commitment are expressed
427 in the self-renewal compartment, supporting a role of *Apc* in controlling early homeostatic fate
428 decision in ISCs. Moreover, transcriptomic profiles provided us with a list of early markers of
429 Wnt oncogenic activation that are exclusively expressed in Apc^{KO} cells, as we show in the case

of *Sox17,* which is undetectable in the Apc^{WT} epithelium, including in ISCs, and could be used to trace aberrant Wnt activation.

Of note, the over-activation of Wnt signaling in ISCs led to an increased number of Myc-expressing cells without increasing the cellular expression of *Myc*, a key mediator of the phenotype associated with *Apc* loss-of-function in intestinal epithelium(40), whose expression coincides with β-catenin signaling in both normal and pre-tumoral crypts. This finding allowed us to conclude that *Myc* is expressed in cells with active Wnt signaling and, reminiscently to its role during development(39), co-operates to the establishment of a crypt-like phenotype in the Apc^{KO} epithelium, but its role in ISCs is not exacerbated upon oncogenic Wnt over-activation.

Alterations in DNA methylation have extensively been proven in advanced tumor stages, and were suspected to play a pivotal role during intestinal tumorigenesis (54,55). However, the confounding cellular heterogeneity of the tissues used for comparison between tumor and healthy profiles has hampered precise conclusions about its actual contribution to cancer initiation. The RRBS profiling of ISCs and early progenitors provided evidences that the oncogenic Wnt activation does not trigger an immediate extensive remodeling of the DNA methylation landscape in the ISC compartment. Instead, *Apc* disruption rapidly produces discrete DNA methylation changes, indicating that focal remodeling of DNA methylation profiles initiates as early as the first oncogenic event, *i.e.* loss of *Apc* function, before becoming more generalized in later stages of the disease. The characterization of CpG-rich genomic regions methylation showed that these changes are rarely found in the close proximity to gene TSSs. Of note, methylation of non CpG-rich regions, as well as other epigenetic marks, may also contribute to the transcriptional and functional dysregulation observed in Apc^{KO} ISCs. However, we show that genes implicated in the signaling pathways governing intestinal cell fate decisions represent preferential targets for altered DNA methylation during early

tumorigenesis. The short timing in our experimental design rules out the possibility that these alterations represent the result of a clonal selection, and rather suggests the existence of a specific program associated with the loss of *Apc* function and Wnt constitutive activation.

Several studies have reported the impact of DNA methylation in controlling cell differentiation (15,19–25), and the activity of *de novo* DNMTs was shown to regulate hematopoietic multipotency and stemness both in homeostasis and cancer (56). The specific role of Dnmt3a and Dnmt3b in intestinal homeostasis awaits further elucidation. However, the fact that these factors are expressed in the ISC compartment, together with the expansion of their pattern of expression in early lesions prompted us to investigate their functional implication in ISCs during intestinal tumorigenesis. Importantly, we show that *Dnmt3a/Dnmt3b* knock-down/inhibition in Apc^{KO} intestinal organotypic cultures reduces the proportion of actively proliferating cells to a homeostatic level comparable with Apc^{WT} organoids, therefore restraining the uncontrolled expansion of Apc^{KO} organoids. Moreover, functional organotypic assays suggest that the activity of *de novo* methyltransferases may contribute to ISC accumulation by impairing their responsiveness to exogenous stimuli controlling the homeostatic balance between self-renewal and differentiation, such as Wnt and BMP signaling upon *Apc* inactivation. BMP signaling has been recently shown to play a crucial role in the commitment of $Lgr5^{+}$ ISCs by repressing the signature associated with stemness without affecting Wnt signaling, therefore preventing ISC outgrowth during homeostasis and regeneration (47). However, we show that Wnt constitutive activation rapidly impairs the responsiveness of ISCs to BMP signals, hence demonstrating an interaction between these pathways in early oncogenesis. More investigation is needed to identify specific and overlapping genomic targets of the two *de novo* DNMTs in the $Lgr5^{+}$ compartment both during homeostasis and tumorigenesis, as recently accomplished in hematopoietic and epidermal stem cells (56,57). This question might be addressed by combining conditional $Dnmt3(a/b)^{Flox}$ and

480 *Apc*^{Flox} alleles with the *Lgr5-Cre*^{ERT2}*-Ires-EGFP* model. Overall, our findings establish a
481 critical effector role for DNA methylation in ISCs, at the onset of the tumor phenotype resulting
482 from *Apc* disruption, and paves the way towards the design of novel strategies suitable to target
483 the tumor stem cell compartment.

484

485

486 **Acknowledgments**

487 This work was supported by ITMO Cancer (Plan Cancer 2009-2013 EPIG201311 to P.J. and
488 M.W.), SIRIC Montpellier Cancer (grant INCa_Inserm_DGOS_12553 to P.J), ARC
489 (SL220110603456 to P.J.), ANR (ANR-14-CE14-0025-01 and ANR-17-CE15-0016-01 to
490 P.J.), INCa (2014-174 and INCA_2018-158 to P.J.), the Labex EpiGenMed (an
491 "Investissements d'avenir" program ANR-10-LABX-12-01 to P.J.), the PJ team is "Equipe
492 Labellisée Ligue contre le Cancer", and the European Research Council (Consolidator grant
493 n°615371 to M.W.). M.B. was supported by Ligue Nationale contre le Cancer. We acknowledge
494 M. Zenati, S. Barahoui and E. Sidot for contribution to the collection of data, J. Pannequin and
495 T. Bouschet for reagents, protocols and advices, C. Perret (Cochin Institute, France) for sharing
496 the *Apc*-mutated mice, the team of S. Fre (Curie Institute, France) for protocols of organotypic
497 culture, F. Gallardo and D. Greuet in the iExplore facility for maintenance of mouse colonies,
498 and C. Duperray in the Montpellier Ressources Imagerie (MRI) facility.

499

500

501

502

503 **REFERENCES**

504 1. Bray F, Ferlay J, Soerjomataram I, Siegel RL, Torre LA, Jemal A. Global cancer statistics 2018:
505 GLOBOCAN estimates of incidence and mortality worldwide for 36 cancers in 185 countries. CA
506 Cancer J Clin. 2018;68:394–424.

507 2. Su LK, Kinzler KW, Vogelstein B, Preisinger AC, Moser AR, Luongo C, et al. Multiple intestinal
508 neoplasia caused by a mutation in the murine homolog of the APC gene. Science.
509 1992;256:668–70.

510 3. Colnot S, Niwa-Kawakita M, Hamard G, Godard C, Le Plenier S, Houbron C, et al. Colorectal
511 cancers in a new mouse model of familial adenomatous polyposis: influence of genetic and
512 environmental modifiers. Lab Invest. 2004;84:1619–30.

4. Barker N, Ridgway RA, van Es JH, van de Wetering M, Begthel H, van den Born M, et al. Crypt stem cells as the cells-of-origin of intestinal cancer. Nature. 2009;457:608–11.

5. Barker N, Bartfeld S, Clevers H. Tissue-resident adult stem cell populations of rapidly self-renewing organs. Cell Stem Cell. 2010;7:656–70.

6. Sansom OJ, Reed KR, Hayes AJ, Ireland H, Brinkmann H, Newton IP, et al. Loss of Apc in vivo immediately perturbs Wnt signaling, differentiation, and migration. Genes Dev. 2004;18:1385–90.

7. Andreu P, Colnot S, Godard C, Gad S, Chafey P, Niwa-Kawakita M, et al. Crypt-restricted proliferation and commitment to the Paneth cell lineage following Apc loss in the mouse intestine. Dev Camb Engl. 2005;132:1443–51.

8. Fearon ER, Vogelstein B. A genetic model for colorectal tumorigenesis. Cell. 1990;61:759–67.

9. Drost J, van Jaarsveld RH, Ponsioen B, Zimberlin C, van Boxtel R, Buijs A, et al. Sequential cancer mutations in cultured human intestinal stem cells. Nature. 2015;521:43–7.

10. Matano M, Date S, Shimokawa M, Takano A, Fujii M, Ohta Y, et al. Modeling colorectal cancer using CRISPR-Cas9-mediated engineering of human intestinal organoids. Nat Med. 2015;21:256–62.

11. Feinberg AP, Vogelstein B. Hypomethylation distinguishes genes of some human cancers from their normal counterparts. Nature. 1983;301:89–92.

12. Kulis M, Esteller M. DNA methylation and cancer. Adv Genet. 2010;70:27–56.

13. Grimm C, Chavez L, Vilardell M, Farrall AL, Tierling S, Böhm JW, et al. DNA-methylome analysis of mouse intestinal adenoma identifies a tumour-specific signature that is partly conserved in human colon cancer. PLoS Genet. 2013;9:e1003250.

14. Bestor TH. The DNA methyltransferases of mammals. Hum Mol Genet. 2000;9:2395–402.

15. Kaaij LTJ, van de Wetering M, Fang F, Decato B, Molaro A, van de Werken HJG, et al. DNA methylation dynamics during intestinal stem cell differentiation reveals enhancers driving gene expression in the villus. Genome Biol. 2013;14:R50.

16. Lin H, Yamada Y, Nguyen S, Linhart H, Jackson-Grusby L, Meissner A, et al. Suppression of intestinal neoplasia by deletion of Dnmt3b. Mol Cell Biol. 2006;26:2976–83.

17. Weis B, Schmidt J, Maamar H, Raj A, Lin H, Tóth C, et al. Inhibition of intestinal tumor formation by deletion of the DNA methyltransferase 3a. Oncogene. 2015;34:1822–30.

18. Linhart HG, Lin H, Yamada Y, Moran E, Steine EJ, Gokhale S, et al. Dnmt3b promotes tumorigenesis in vivo by gene-specific de novo methylation and transcriptional silencing. Genes Dev. 2007;21:3110–22.

19. Jackson M, Krassowska A, Gilbert N, Chevassut T, Forrester L, Ansell J, et al. Severe global DNA hypomethylation blocks differentiation and induces histone hyperacetylation in embryonic stem cells. Mol Cell Biol. 2004;24:8862–71.

549 20. Smith ZD, Meissner A. DNA methylation: roles in mammalian development. Nat Rev Genet.
550 2013;14:204–20.

551 21. Meissner A, Mikkelsen TS, Gu H, Wernig M, Hanna J, Sivachenko A, et al. Genome-scale DNA
552 methylation maps of pluripotent and differentiated cells. Nature. 2008;454:766–70.

553 22. Ji H, Ehrlich LIR, Seita J, Murakami P, Doi A, Lindau P, et al. Comprehensive methylome map of
554 lineage commitment from haematopoietic progenitors. Nature. 2010;467:338–42.

555 23. Bock C, Beerman I, Lien W-H, Smith ZD, Gu H, Boyle P, et al. DNA methylation dynamics during in
556 vivo differentiation of blood and skin stem cells. Mol Cell. 2012;47:633–47.

557 24. Cortese R, Lewin J, Bäckdahl L, Krispin M, Wasserkort R, Eckhardt F, et al. Genome-wide screen
558 for differential DNA methylation associated with neural cell differentiation in mouse. PloS One.
559 2011;6:e26002.

560 25. Sheaffer KL, Kim R, Aoki R, Elliott EN, Schug J, Burger L, et al. DNA methylation is required for the
561 control of stem cell differentiation in the small intestine. Genes Dev. 2014;28:652–64.

562 26. Sato T, Vries RG, Snippert HJ, van de Wetering M, Barker N, Stange DE, et al. Single Lgr5 stem
563 cells build crypt–villus structures in vitro without a mesenchymal niche. Nature. 2009;459:262–
564 5.

565 27. Onuma K, Ochiai M, Orihashi K, Takahashi M, Imai T, Nakagama H, et al. Genetic reconstitution
566 of tumorigenesis in primary intestinal cells. Proc Natl Acad Sci U S A. 2013;110:11127–32.

567 28. Gerbe F, van Es JH, Makrini L, Brulin B, Mellitzer G, Robine S, et al. Distinct ATOH1 and Neurog3
568 requirements define tuft cells as a new secretory cell type in the intestinal epithelium. J Cell
569 Biol. 2011;192:767–80.

570 29. Barker N, van Es JH, Kuipers J, Kujala P, van den Born M, Cozijnsen M, et al. Identification of stem
571 cells in small intestine and colon by marker gene Lgr5. Nature. 2007;449:1003–7.

572 30. Korinek V, Barker N, Moerer P, van Donselaar E, Huls G, Peters PJ, et al. Depletion of epithelial
573 stem-cell compartments in the small intestine of mice lacking Tcf-4. Nat Genet. 1998;19:379–
574 83.

575 31. van Es JH, Haegebarth A, Kujala P, Itzkovitz S, Koo B-K, Boj SF, et al. A Critical Role for the Wnt
576 Effector Tcf4 in Adult Intestinal Homeostatic Self-Renewal. Mol Cell Biol. 2012;32:1918–27.

577 32. Muñoz J, Stange DE, Schepers AG, van de Wetering M, Koo B-K, Itzkovitz S, et al. The Lgr5
578 intestinal stem cell signature: robust expression of proposed quiescent “+4” cell markers.
579 EMBO J. 2012;31:3079–91.

580 33. Merlos-Suárez A, Barriga FM, Jung P, Iglesias M, Céspedes MV, Rossell D, et al. The intestinal
581 stem cell signature identifies colorectal cancer stem cells and predicts disease relapse. Cell
582 Stem Cell. 2011;8:511–24.

583 34. van Es JH, Jay P, Gregorieff A, van Gijn ME, Jonkheer S, Hatzis P, et al. Wnt signalling induces
584 maturation of Paneth cells in intestinal crypts. Nat Cell Biol. 2005;7:381–6.

35. Ng AY-N, Waring P, Ristevski S, Wang C, Wilson T, Pritchard M, et al. Inactivation of the transcription factor Elf3 in mice results in dysmorphogenesis and altered differentiation of intestinal epithelium. Gastroenterology. 2002;122:1455–66.

36. San Roman AK, Tovaglieri A, Breault DT, Shivdasani RA. Distinct Processes and Transcriptional Targets Underlie CDX2 Requirements in Intestinal Stem Cells and Differentiated Villus Cells. Stem Cell Rep. 2015;5:673–81.

37. Gierl MS, Karoulias N, Wende H, Strehle M, Birchmeier C. The zinc-finger factor Insm1 (IA-1) is essential for the development of pancreatic beta cells and intestinal endocrine cells. Genes Dev. 2006;20:2465–78.

38. Gerbe F, Sidot E, Smyth DJ, Ohmoto M, Matsumoto I, Dardalhon V, et al. Intestinal epithelial tuft cells initiate type 2 mucosal immunity to helminth parasites. Nature. 2016;529:226–30.

39. Bettess MD, Dubois N, Murphy MJ, Dubey C, Roger C, Robine S, et al. c-Myc Is Required for the Formation of Intestinal Crypts but Dispensable for Homeostasis of the Adult Intestinal Epithelium. Mol Cell Biol. 2005;25:7868–78.

40. Sansom OJ, Meniel VS, Muncan V, Phesse TJ, Wilkins JA, Reed KR, et al. Myc deletion rescues Apc deficiency in the small intestine. Nature. 2007;446:676–9.

41. Berman BP, Weisenberger DJ, Aman JF, Hinoue T, Ramjan Z, Liu Y, et al. Regions of focal DNA hypermethylation and long-range hypomethylation in colorectal cancer coincide with nuclear lamina-associated domains. Nat Genet. 2011;44:40–6.

42. Forn M, Díez-Villanueva A, Merlos-Suárez A, Muñoz M, Lois S, Carriò E, et al. Overlapping DNA Methylation Dynamics in Mouse Intestinal Cell Differentiation and Early Stages of Malignant Progression. PLoS ONE [Internet]. 2015 [cited 2017 Apr 3];10. Available from: http://www.ncbi.nlm.nih.gov/pmc/articles/PMC4416816/

43. Howard G, Eiges R, Gaudet F, Jaenisch R, Eden A. Activation and transposition of endogenous retroviral elements in hypomethylation induced tumors in mice. Oncogene. 2008;27:404–8.

44. Bakshi A, Kim J. Retrotransposon-based profiling of mammalian epigenomes: DNA methylation of IAP LTRs in embryonic stem, somatic and cancer cells. Genomics. 2014;104:538–44.

45. Vermeulen L, De Sousa E Melo F, van der Heijden M, Cameron K, de Jong JH, Borovski T, et al. Wnt activity defines colon cancer stem cells and is regulated by the microenvironment. Nat Cell Biol. 2010;12:468–76.

46. Whissell G, Montagni E, Martinelli P, Hernando-Momblona X, Sevillano M, Jung P, et al. The transcription factor GATA6 enables self-renewal of colon adenoma stem cells by repressing BMP gene expression. Nat Cell Biol. 2014;16:695–707.

47. Qi Z, Li Y, Zhao B, Xu C, Liu Y, Li H, et al. BMP restricts stemness of intestinal $Lgr5^+$ stem cells by directly suppressing their signature genes. Nat Commun. 2017;8:13824.

48. Haramis A-PG, Begthel H, van den Born M, van Es J, Jonkheer S, Offerhaus GJA, et al. De novo crypt formation and juvenile polyposis on BMP inhibition in mouse intestine. Science. 2004;303:1684–6.

623 49. Davis H, Irshad S, Bansal M, Rafferty H, Boitsova T, Bardella C, et al. Aberrant epithelial GREM1
624 expression initiates colonic tumorigenesis from cells outside the stem cell niche. Nat Med.
625 2015;21:62–70.

626 50. Kuck D, Caulfield T, Lyko F, Medina-Franco JL. Nanaomycin A selectively inhibits DNMT3B and
627 reactivates silenced tumor suppressor genes in human cancer cells. Mol Cancer Ther.
628 2010;9:3015–23.

629 51. Yan KS, Janda CY, Chang J, Zheng GXY, Larkin KA, Luca VC, et al. Non-equivalence of Wnt and R-
630 spondin ligands during Lgr5(+) intestinal stem-cell self-renewal. Nature. 2017;545:238–42.

631 52. Sato T, Stange DE, Ferrante M, Vries RGJ, Van Es JH, Van den Brink S, et al. Long-term expansion
632 of epithelial organoids from human colon, adenoma, adenocarcinoma, and Barrett's
633 epithelium. Gastroenterology. 2011;141:1762–72.

634 53. Grün D, Lyubimova A, Kester L, Wiebrands K, Basak O, Sasaki N, et al. Single-cell messenger RNA
635 sequencing reveals rare intestinal cell types. Nature. 2015;525:251–5.

636 54. Feinberg AP, Vogelstein B. Alterations in DNA methylation in human colon neoplasia. Semin Surg
637 Oncol. 1987;3:149–51.

638 55. Timp W, Feinberg AP. Cancer as a dysregulated epigenome allowing cellular growth advantage at
639 the expense of the host. Nat Rev Cancer. 2013;13:497–510.

640 56. Challen GA, Sun D, Mayle A, Jeong M, Luo M, Rodriguez B, et al. Dnmt3a and Dnmt3b have
641 overlapping and distinct functions in hematopoietic stem cells. Cell Stem Cell. 2014;15:350–64.

642 57. Rinaldi L, Datta D, Serrat J, Morey L, Solanas G, Avgustinova A, et al. Dnmt3a and Dnmt3b
643 Associate with Enhancers to Regulate Human Epidermal Stem Cell Homeostasis. Cell Stem Cell.
644 2016;19:491–501.

645

646 **FIGURE 1. Expansion of the self-renewal compartment consequent to *Apc* loss-**
647 **of-function in Lgr5^{+} ISCs. A,** Representative flow cytometry analyses of GFP content in
648 dissociated intestinal epithelium from *$Apc^{+/+}$* : , *$Apc^{LoxP/+}$: or $Apc^{LoxP/LoxP}$* : *Lgr5-Cre^{ERT2}-ires-*
649 *eGFP* or control mice 15 days after the initial administration of tamoxifen and **B,** flow
650 cytometry quantification of the % of eGFP^{+} cells; bars represent mean ± SEM of n= 6 *$Apc^{+/+}$,*
651 *5 $Apc^{LoxP/+}$ and 7 $Apc^{LoxP/LoxP}$ mice;* **p*<0.05. **C**, clone formation ability of GFP^{+} isolated cells
652 quantified as the number of resulting multicellular organoids; bars represent mean ± SEM of
653 n=16 wells seeded with equal number of *Apc^{WT}* or *Apc^{KO}* FACS-sorted GFP^{+} cells from an
654 *$Apc^{+/+}$* or *$Apc^{LoxP/LoxP}$* mouse; ***p*<0.01. **D,** representative immunofluorescence fields of
655 proximal intestines showing the increased proportion of Olfm4^{+} cells and **E,** Sox9^{+} cells in
656 *$Apc^{LoxP/LoxP}$*- crypts as compared to control crypts from *$Apc^{+/+}$; Lgr5-Cre^{ERT2}-ires-eGFP* mice
657 (scale bar = 10μm) . **F**, representative immunofluorescence fields of proximal intestines from
658 *$Apc^{+/+}$ or $Apc^{LoxP/LoxP}$ Lgr5-Cre^{ERT2}-ires-eGFP* mice (scale bar = 10μm) used to quantify the %

of **G,** total crypt BrdU$^+$ cells or **H**, % of BrdU$^+$/GFP$^+$. **I**, quantification of the flow cytometry analyses on the distribution of GFP$^+$ cells in the cell cycle according to the amount of DNA; bars represent mean ± SEM of integration of multiple technical replicates from 3 (7, 7, 5 replicates) *Apc*$^{+/+}$*-, 4* (4, 5, 5, 2 replicates) *Apc*$^{LoxP/+}$- or 4 (5 replicates each) *Apc*$^{LoxP/LoxP}$- mice respectively*;* ***p<0.001 **J**) BrdU$^+$/GFP$^+$ cells in physical contact with at least 1 Lyz$^+$ Paneth cell per intestinal crypt; nuclei are counterstained with Hoechst; bars for **G**, **H** and **J** represent integration mean ± SEM of n=43 (14, 15, 14), 45 (15, 15, 15) and 41 (15, 11, 15) crypts from 3 *Apc*$^{+/+}$*, 3 Apc*$^{LoxP/+}$*or 3 Apc*$^{LoxP/LoxP}$ mice respectively*;* (*Apc*^{WT} vs. *Apc*^{KO}) or Mann-Whitney (*Apc*^{WT} vs. *Apc*^{HET} *and Apc*^{HET} vs. *Apc*^{KO}); *p<0.05.

FIGURE 2. Wnt perturbation is associated with aberrant gene expression in Lgr5$^+$ ISCs and impaired molecular cell fate. A, volcano plots representing the changes in gene expression and adjusted *p-value*s for the different comparisons. Significantly differentially expressed genes (FDR adjusted p<0.01) are represented in red; data represent the results of RNA-seq analyses from 4 animals per genotype. **B**, GSEA analyses showing the enrichment of gene sets associated with Wnt activation, cell cycle progression, GFP^{high} ISCs[39], terminally differentiated epithelium[40] and GFP-low TA cells[39]; ES, enrichment score; NES, normalized enrichment score; positive and negative ES indicate enrichment in *Apc*^{WT}- or *Apc*^{KO} Lgr5-GFP$^+$ profiles respectively; statistically significant correlations (FDR-adjusted p<0.05) are highlighted in green. **C**, examples of makers associated to ISCs identity or **D**, epithelial commitment and post-mitotic differentiation as by RNAseq analyses; normalized gene expression is represented as Fragments per kilo-base per million mapped reads (FPKM); ***FDR adjusted p<0.001, ** FDR adjusted p<0.01. Representative immunofluorescence fields of proximal intestines showing the expression of **E,** Elf3, **F**, Cdx2, **G**, Insm1 and **H,** Pou2f3 in GFP$^+$ cells from *Apc*$^{+/+}$*; Lgr5-Cre*^{ERT2}*-ires-eGFP* control crypts (scale bar = 10µm); arrows indicate GFP$^+$ cells at CBC anatomical location.

FIGURE 3. An early and specific DNA methylation program associated with Wnt constitutive activation in Lgr5$^+$-ISCs. A, cluster dendrogram showing similarity between the CpG methylation profiles measured by RRBS in Lgr5-GFP$^+$ FACS-sorted cells. **B**, density scatter plots representing the correlation between CpG methylation scores (from 0 to 100%) in Lgr5-GFP$^+$ cells; differentially methylated CpGs (qValue<0.01) are shown in red. **C**, Distribution of the number of DMRs according to the extent of methylation change (%) in *Apc*^{HET} (top chart) and *Apc*^{KO} (bottom chart) as compared to *Apc*^{WT} Lgr5-GFP$^+$ cells; negative

and positive values represent hypo- and hypermethylated regions respectively. **D**, heatmap with clustering showing the individual methylation values for DMR in Apc^{KO} and Apc^{WT} cells. **E**, distribution of distance to the closest gene TSS of the hyper- and hypomethylated DMRs found in Apc^{KO} compared to Apc^{WT} Lgr5-eGFP^{+}. **F**, Methylation of different families of transposable elements in $Lgr5^{+}$ cells. **G,** GSEA analyses showing the absence of specific methylation patterns in promoter regions or DMRs associated with sets of genes defining ISCs identity or terminally differentiated epithelium (FDR adjusted $p<0.05$). All data represent the results of RRBS analyses from 4 animals per genotype.

FIGURE 4. *De novo* DNA methylation can rescue the impaired ISC commitment and proliferation in Apc^{KO} mini-guts. A and **C,** expression of Dnmt3a and Dnmt3b as by RNAseq data and **B** and **D,** representative immunofluorescence fields of Apc^{WT}- (top panels) or Apc^{KO}-$Lgr5$-Cre^{ERT2} crypts and adenomatous (bottom panels) $Apc^{\Delta 14/+}$ intestinal epithelium, showing the pattern of expression of Dnmt3a and Dnmt3b during homeostatic disruption and adenoma formation (scale bar = 10µm). **E**, representative immunofluorescences showing the expansion of the Sox9^{+} ISC compartment in Apc^{KO} organoids (scale bar = 10µm). **F**, proliferation of Apc^{WT} and Apc^{KO} organoids expressing control- or double-ShRNA as the % of Ki67^{+} cells; bars represent mean ± SEM of integration of multiple organoids from 2 independently-derived clones per condition; n=19 (9 and 10 organoids) control-Apc^{WT}, 27 (12 and 15) double Sh-Apc^{WT}, 21 (6 and 15) control-Apc^{KO}, 16 (6 and 10) double Sh-Apc^{KO} oganoids; ***p<0.001. **G**, Representative clonogenic assay performed by seeding an equivalent number of organoids corresponding to 40 000 Apc^{KO} cells transduced with NT/NT- or Dnmt3a/b-shRNA. **H**, proliferation of Apc^{WT} and Apc^{KO} organoids treated with Nanaomycin-A or 5-Azacytidine, expressed as the % of KI67^{+} cells; bars represent mean ± SEM of integration of multiple organoids from independent organoid models per condition; n= 8 (5 and 3 organoids) untreated control, 7 (4 and 3) 5-Azacytidine-, 7 (4 and 3) Nanaomycin-A-treated Apc^{WT} and 27 (6, 6, 15) untreated, 18 (5, 4, 9) 5-Azacytidine-treated, 15 (4, 5, 6) Nanaomycin-A-treated Apc^{KO} organoids; *p-value* as determined by t-tests (with Welch's correction when needed), **$p<0.01$, ***$p<0.001$. **I**, RT-PCR products in representative organotypic models per genotype confirming the dynamics of the expression of genes belonging to Wnt (*Axin2*, *Nfatc2*, *Prkca* and *Vangl1*) and BMP signaling pathways (*Smad6*, *Inhbb* and *Smad6*) in *Villin*-Cre^{ERT2} miniguts in response to *Apc* deletion. *Actb* expression is presented as an endogenous loading control.

FIGURE 5. *De novo* Dnmts function is implicated in the reduced responsiveness to homeostatic stimuli after *Apc* inactivation. A) Representative brightfield images of Apc^{KO} organoids expressing control- or double-ShRNA, showing the size of spheroids in response of Dnmt3a/3b knockdown in presence or absence of Rspondin-1 in the culture medium (scale bar = 50µm). **B**, quantifications showing that Dnmt3a/3b knock-down reduces the size of Apc^{KO} organoids, which is further accentuated by the depletion of Rspo from the medium; bars represent mean ± SEM of n=90 organoids (3 serial passaging, 30 replicates each) per condition; ***p<0.001. **C**, Representative brightfield images of crypt-like structure formation in Apc^{KO} organoids expressing Dnmt3a/3b-ShRNA compared to controls after Noggin withdrawal and further stimulation with rBMP2 (scale bar = 50µm). **D**, quantifications showing that Nanaomycin-A treatment reduces the clonogenic ability Apc^{KO} cells to form organoids in the presence of rBM2 stimulation; bars represent mean ± SEM of n=20 control and 20 Nanaomycin-A-treated wells from a single representative experiment. **E**, Representative brightfield images of Apc^{KO} spheroids in response to Nanaomycin-A alone or Nanaomycin-A in combination with the LDN193189 Alk-pSmad1/5/8 BMP inhibitor (scale bar = 50µm), and **F**, quantification of the spheroid size on multiple spheres in the control and treatment conditions; bars represent mean ± SEM of integration of multiple organoids from 2 independent organoid models per condition; n= 61 (30 and 31 spheroids) control, 66 (33 and 33) Nanaomycin-A-treated and 72 (35 and 37) Nanaomycin-A- in combination with LDN193189-treated spheroids; *p-value* as determined by Mann-Whitney *U-test*, ***p<0.001 **G**) Cartoon illustrating the impaired responsiveness to environmental differentiation stimuli, leading to aberrant spheroid morphology in intestinal epithelial organoids after *Apc* inactivation; inhibition of Dnmt3a/3b concomitant to *Apc* deletion prevents this impairment with recovery of a crypt-like morphology.

Figure 1

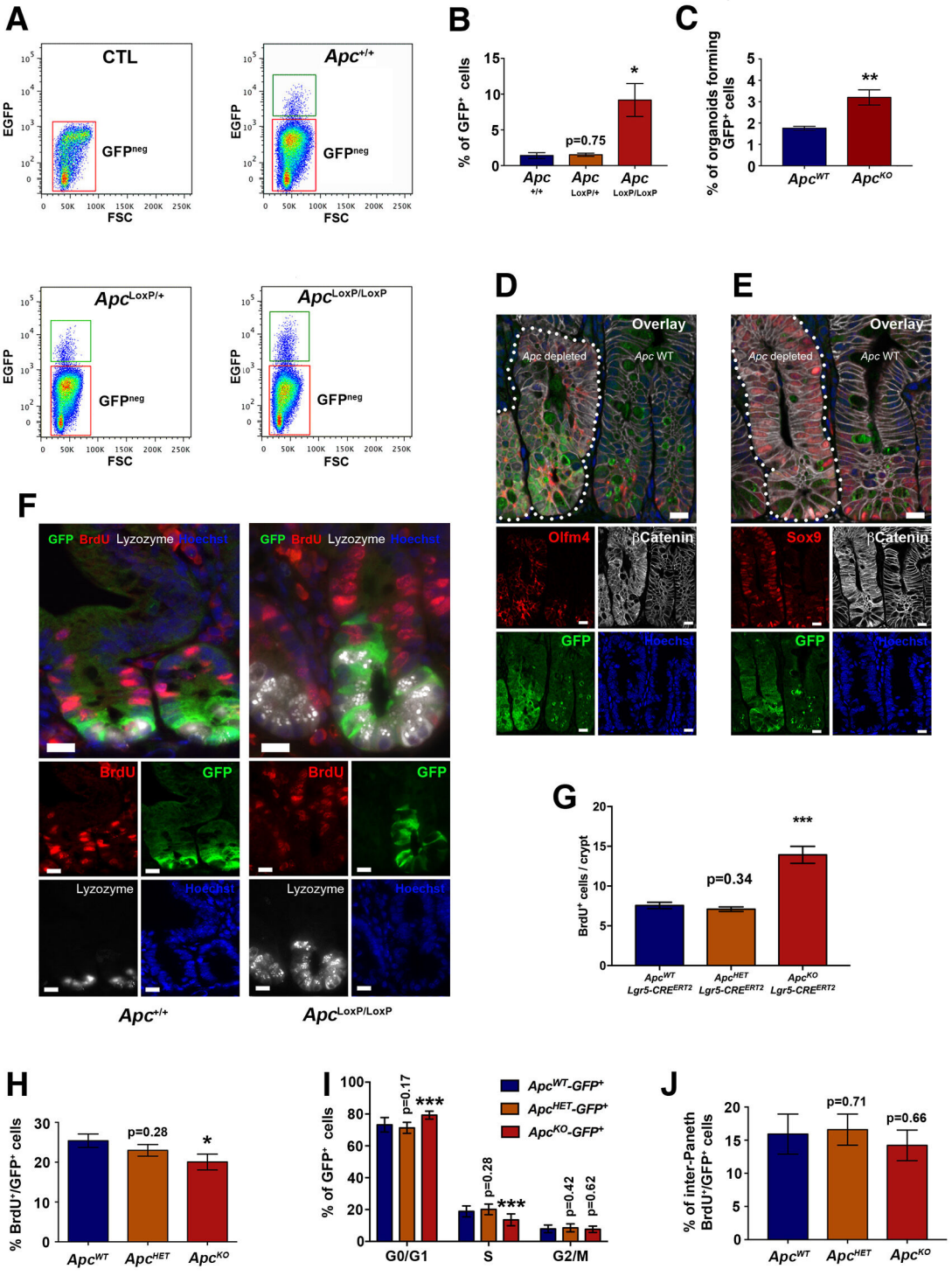
A
CTL
Apc+/+
ApcLoxP/+
ApcLoxP/LoxP
EGFP
FSC
GFPneg
B
% of GFP+ cells
p=0.75
Apc +/+
Apc LoxP/+
Apc LoxP/LoxP
C
% of organoids forming GFP+ cells
ApcWT
ApcKO
D
E
Overlay
Apc depleted
Apc WT
Olfm4
Sox9
βCatenin
GFP
Hoechst
F
GFP BrdU Lyzoxyme Hoechst
BrdU
Lyzoxyme
Apc+/+
ApcLoxP/LoxP
G
BrdU+ cells / crypt
p=0.34
ApcWT Lgr5-CREERT2
ApcHET Lgr5-CREERT2
ApcKO Lgr5-CREERT2
H
% BrdU+/GFP+ cells
p=0.28
ApcWT
ApcHET
ApcKO
I
% of GFP+ cells
ApcWT-GFP+
ApcHET-GFP+
ApcKO-GFP+
p=0.17
p=0.28
p=0.42
p=0.62
G0/G1
S
G2/M
J
% of inter-Paneth BrdU+/GFP+ cells
p=0.71
p=0.66

Figure 2

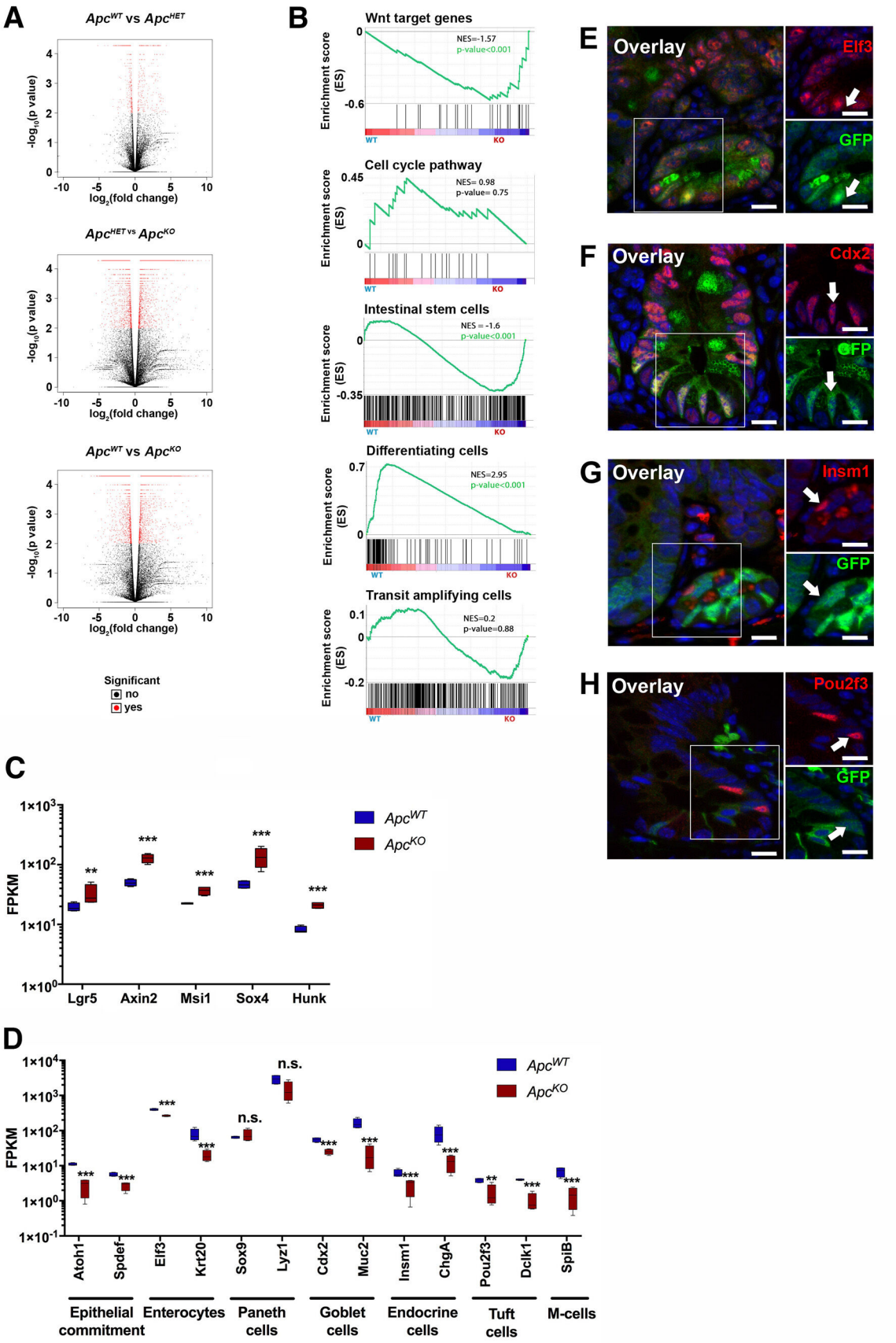
A
Apc^WT vs Apc^HET
Apc^HET vs Apc^KO
Apc^WT vs Apc^KO
-log10(p value)
log2(fold change)
Significant
no
yes
B
Wnt target genes
NES=-1.57
p-value<0.001
Cell cycle pathway
NES= 0.98
p-value= 0.75
Intestinal stem cells
NES = -1.6
p-value<0.001
Differentiating cells
NES=2.95
p-value<0.001
Transit amplifying cells
NES=0.2
p-value=0.88
Enrichment score (ES)
WT
KO
C
FPKM
Apc^WT
Apc^KO
Lgr5
Axin2
Msi1
Sox4
Hunk
D
FPKM
n.s.
Atoh1
Spdef
Elf3
Krt20
Sox9
Lyz1
Cdx2
Muc2
Insm1
ChgA
Pou2f3
Dclk1
SpiB
Epithelial commitment
Enterocytes
Paneth cells
Goblet cells
Endocrine cells
Tuft cells
M-cells
E
Overlay
Elf3
GFP
F
Overlay
Cdx2
GFP
G
Overlay
Insm1
GFP
H
Overlay
Pou2f3
GFP

Figure 3

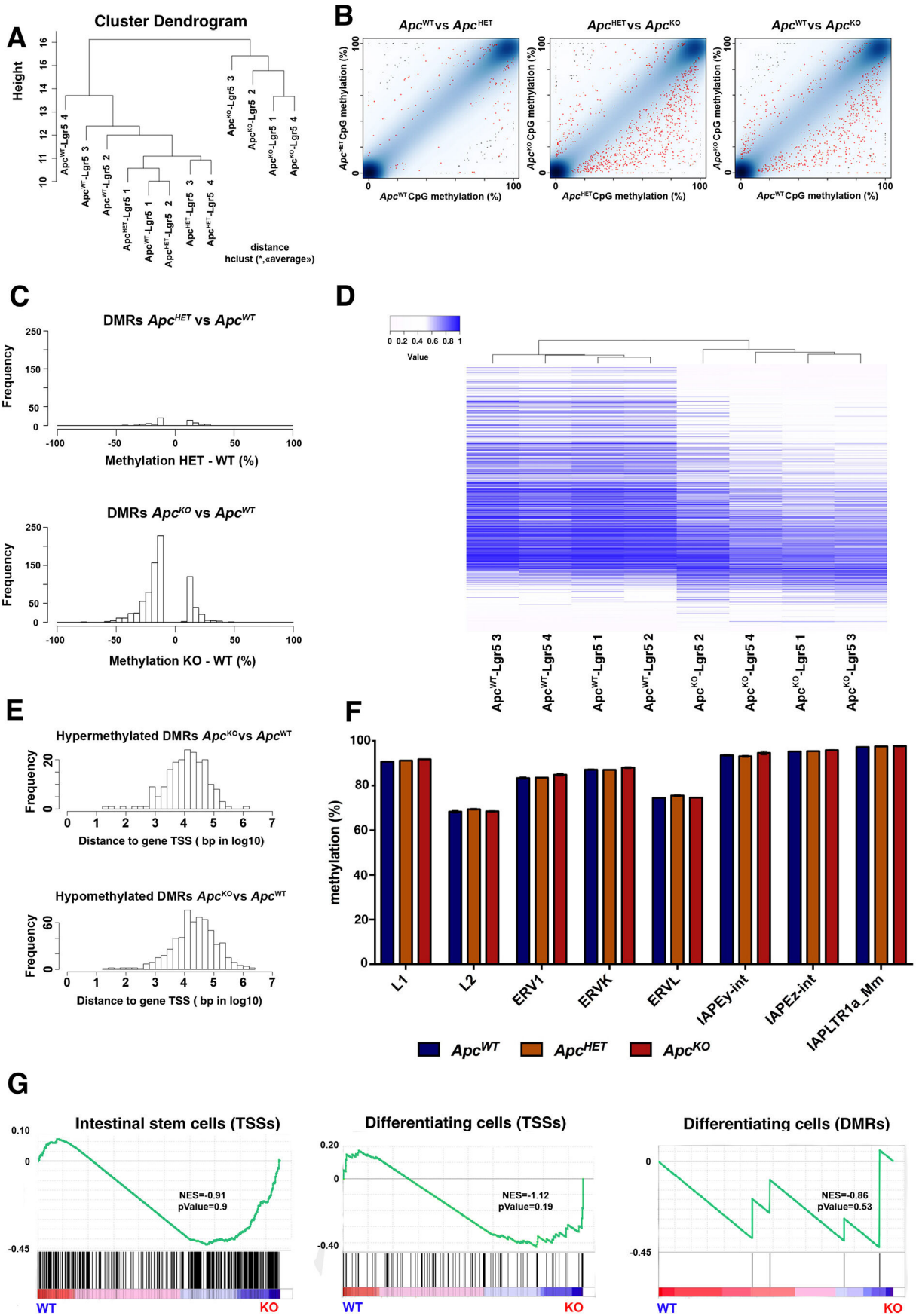
A
Cluster Dendrogram
Height
distance
hclust (*,«average»)
B
ApcWT vs ApcHET
ApcHET vs ApcKO
ApcWT vs ApcKO
ApcHET CpG methylation (%)
ApcWT CpG methylation (%)
ApcKO CpG methylation (%)
C
DMRs ApcHET vs ApcWT
Frequency
Methylation HET - WT (%)
DMRs ApcKO vs ApcWT
Methylation KO - WT (%)
D
Value
E
Hypermethylated DMRs ApcKO vs ApcWT
Distance to gene TSS (bp in log10)
Hypomethylated DMRs ApcKO vs ApcWT
F
methylation (%)
L1
L2
ERV1
ERVK
ERVL
IAPEy-int
IAPEz-int
IAPLTR1a_Mm
ApcWT
ApcHET
ApcKO
G
Intestinal stem cells (TSSs)
NES=-0.91
pValue=0.9
Differentiating cells (TSSs)
NES=-1.12
pValue=0.19
Differentiating cells (DMRs)
NES=-0.86
pValue=0.53
WT
KO

Figure 4

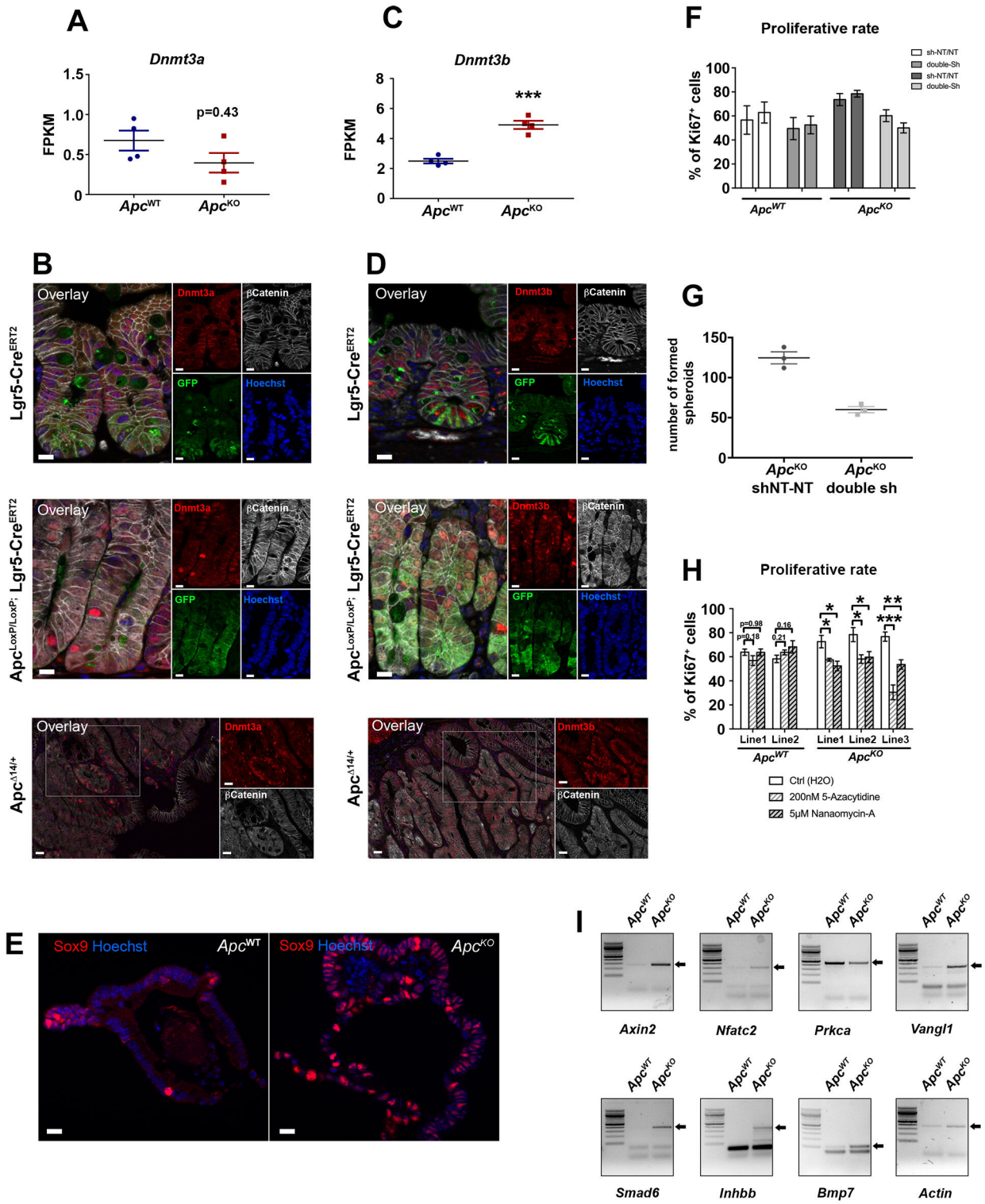
A
Dnmt3a
FPKM
p=0.43
ApcWT
ApcKO
C
Dnmt3b
FPKM
***
ApcWT
ApcKO
F
Proliferative rate
% of Ki67+ cells
sh-NT/NT
double-Sh
sh-NT/NT
double-Sh
ApcWT
ApcKO
B
D
Lgr5-CreERT2
ApcLoxP/LoxP; Lgr5-CreERT2
ApcΔ14/+
Overlay
Dnmt3a
Dnmt3b
βCatenin
GFP
Hoechst
G
number of formed spheroids
ApcKO shNT-NT
ApcKO double sh
H
Proliferative rate
% of Ki67+ cells
p=0.98
p=0.18
0.16
0.21
Line1
Line2
Line3
ApcWT
ApcKO
Ctrl (H2O)
200nM 5-Azacytidine
5μM Nanaomycin-A
E
Sox9 Hoechst
ApcWT
ApcKO
I
Axin2
Nfatc2
Prkca
Vangl1
Smad6
Inhbb
Bmp7
Actin

Figure 5

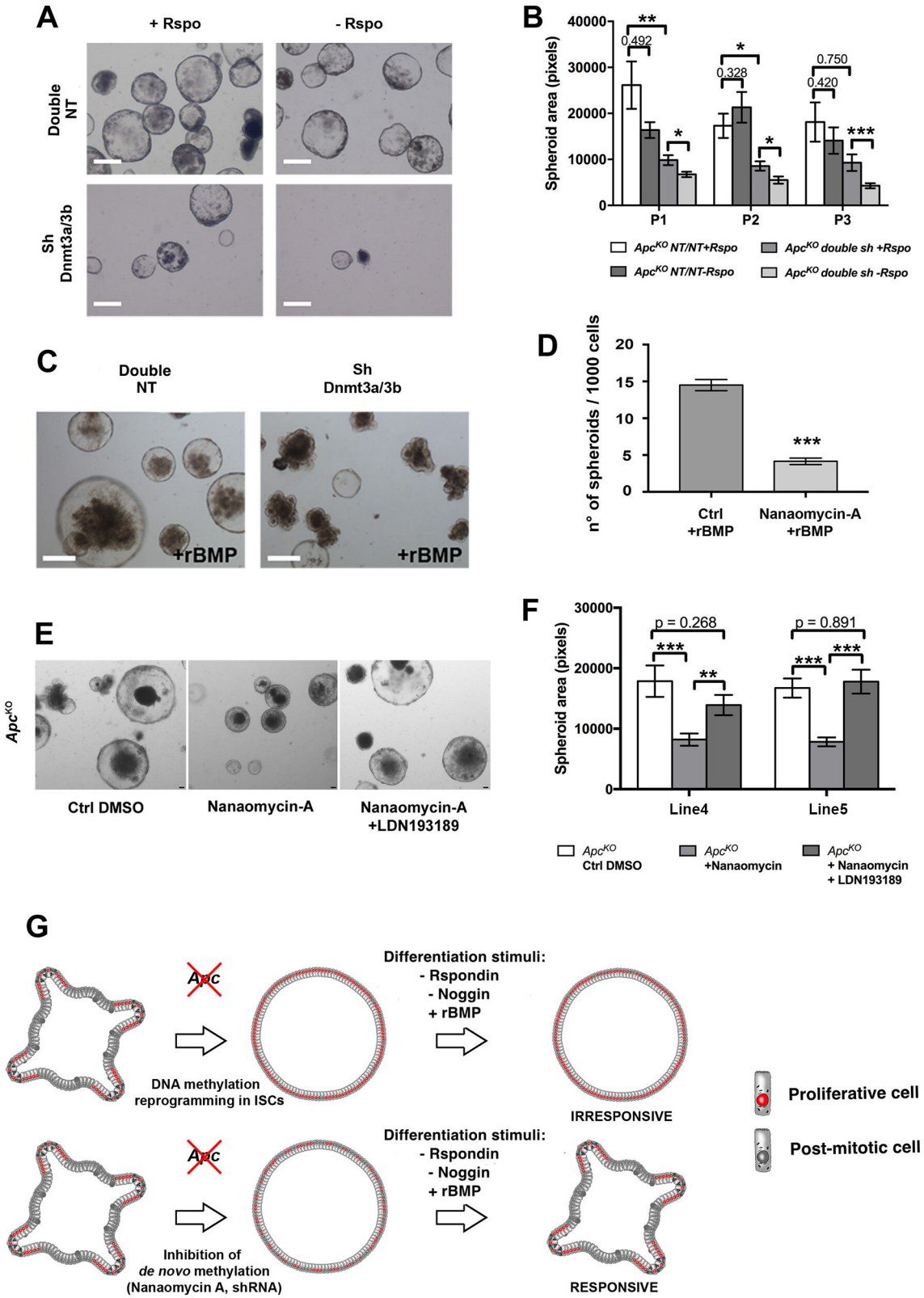
A
+ Rspo
- Rspo
Double NT
Sh Dnmt3a/3b
B
Spheroid area (pixels)
40000
30000
20000
10000
0
0.492
0.328
0.420
0.750
P1
P2
P3
ApcKO NT/NT+Rspo
ApcKO NT/NT-Rspo
ApcKO double sh +Rspo
ApcKO double sh -Rspo
C
Double NT
Sh Dnmt3a/3b
+rBMP
+rBMP
D
n° of spheroids / 1000 cells
20
15
10
5
0
Ctrl +rBMP
Nanaomycin-A +rBMP
E
ApcKO
Ctrl DMSO
Nanaomycin-A
Nanaomycin-A +LDN193189
F
Spheroid area (pixels)
30000
20000
10000
0
p = 0.268
p = 0.891
Line4
Line5
ApcKO Ctrl DMSO
ApcKO +Nanaomycin
ApcKO + Nanaomycin + LDN193189
G
Apc
DNA methylation reprogramming in ISCs
Differentiation stimuli:
- Rspondin
- Noggin
+ rBMP
IRRESPONSIVE
Inhibition of de novo methylation (Nanaomycin A, shRNA)
RESPONSIVE
Proliferative cell
Post-mitotic cell

Supplemental Figure 1

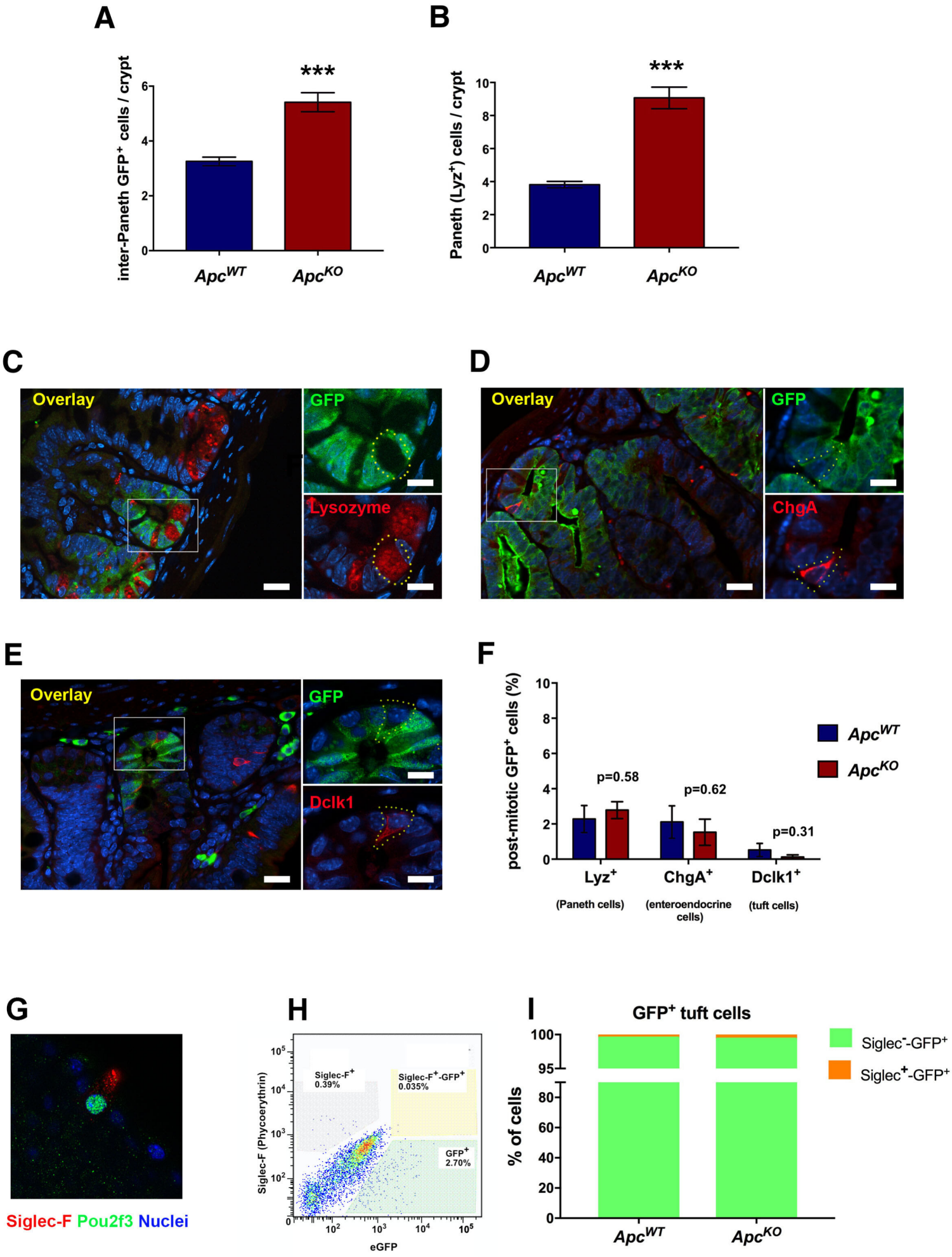

Supplemental Figure 2

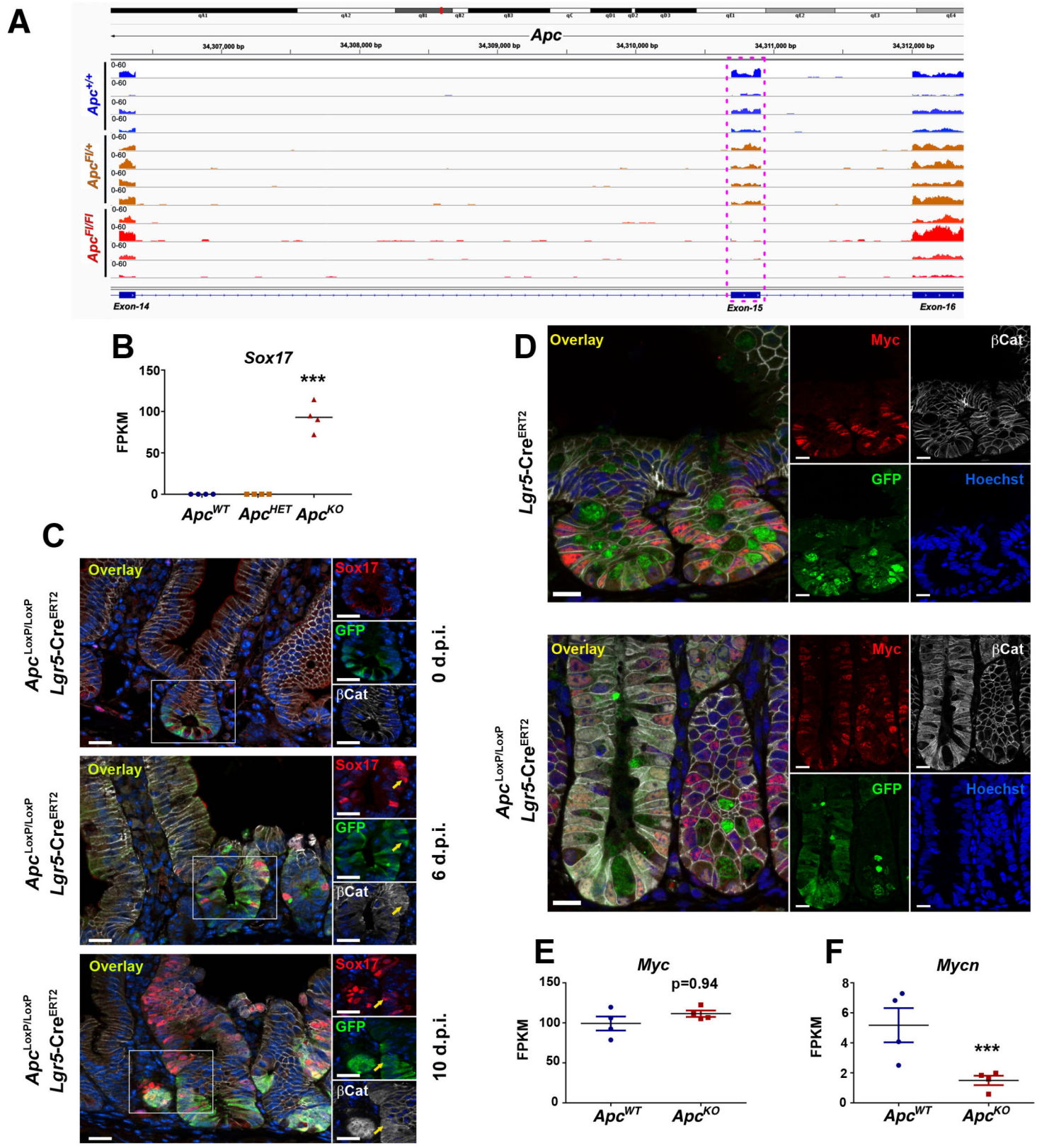

Supplemental Figure 3

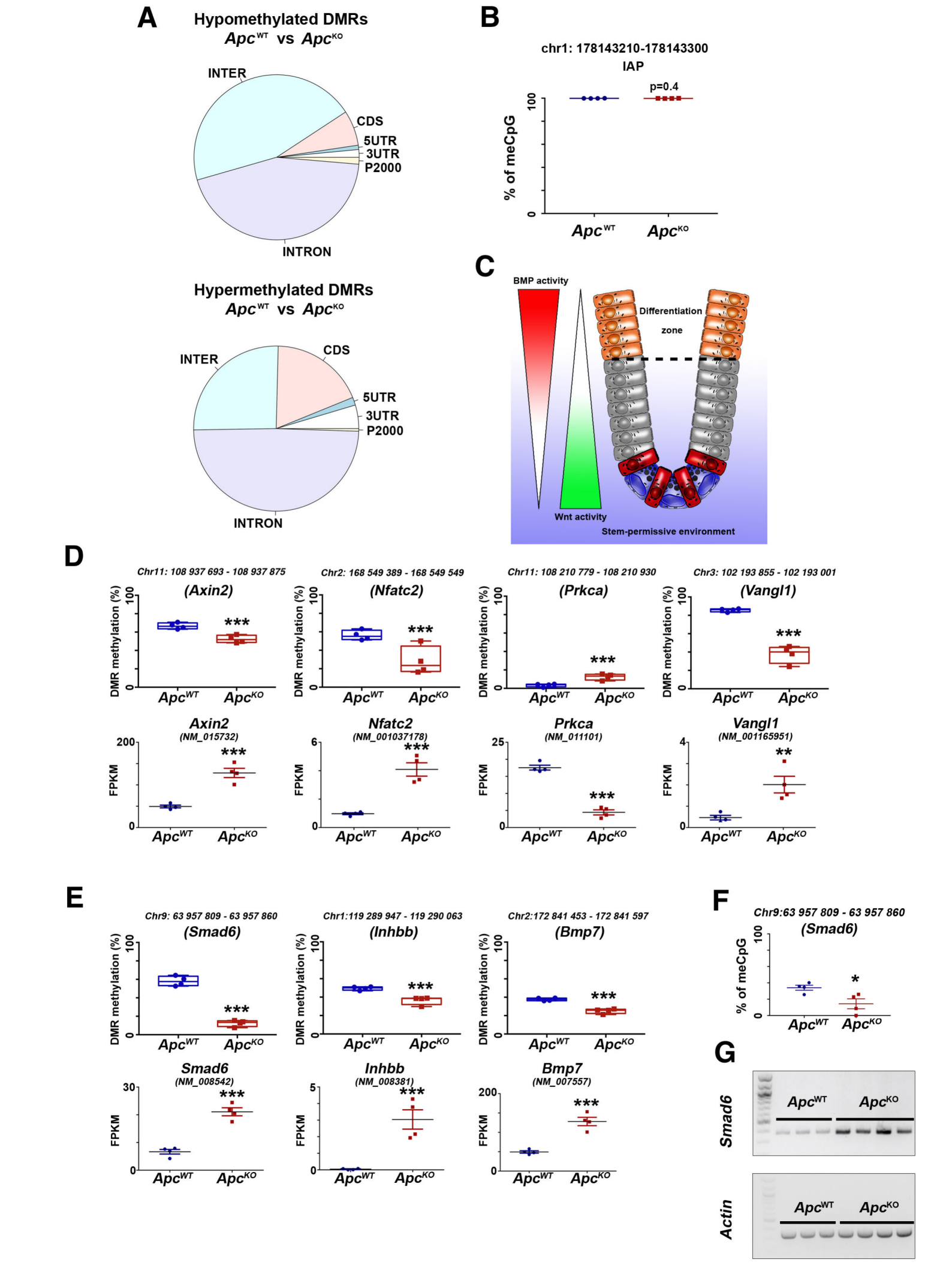

Supplemental Figure 4

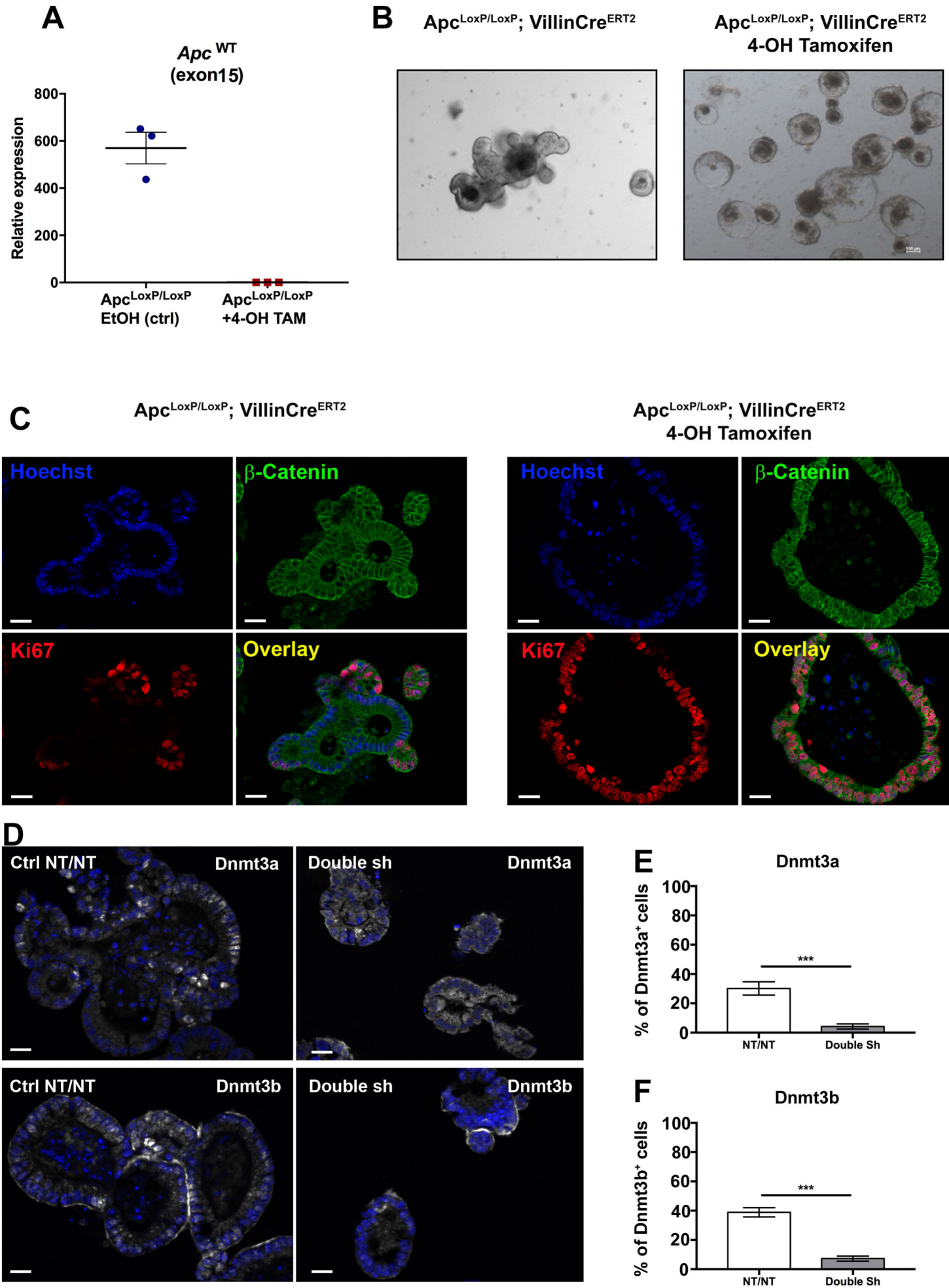

Supplemental Figure 5